

Variational Image Reconstruction for Dynamic High Resolution Photoacoustic Tomography

Felix Lucka¹, Marta Betcke¹, Nam Huynh², Edward Zhang², Paul Beard², Ben Cox² and Simon Arridge¹

1) Department of Computer Science 2) Department of Medical Physics
University College London, WC1E 6BT London, UK

contact: f.lucka@ucl.ac.uk



Compressed Photoacoustic Sensing

Current PAT systems offer either exquisite image quality or high frame rates but not both. As the spatio-temporal complexity of many absorbing tissue structures is rather low, the data recorded is often highly redundant. Therefore, developing systems that only sense the non-redundant part of the data can increase the acquisition speed. We examine the acceleration of sequential Fabry-Pérot scanners (Fig 1) by random single-point (rSP) or patterned interrogation (PI) sub-sampling (Fig 2).

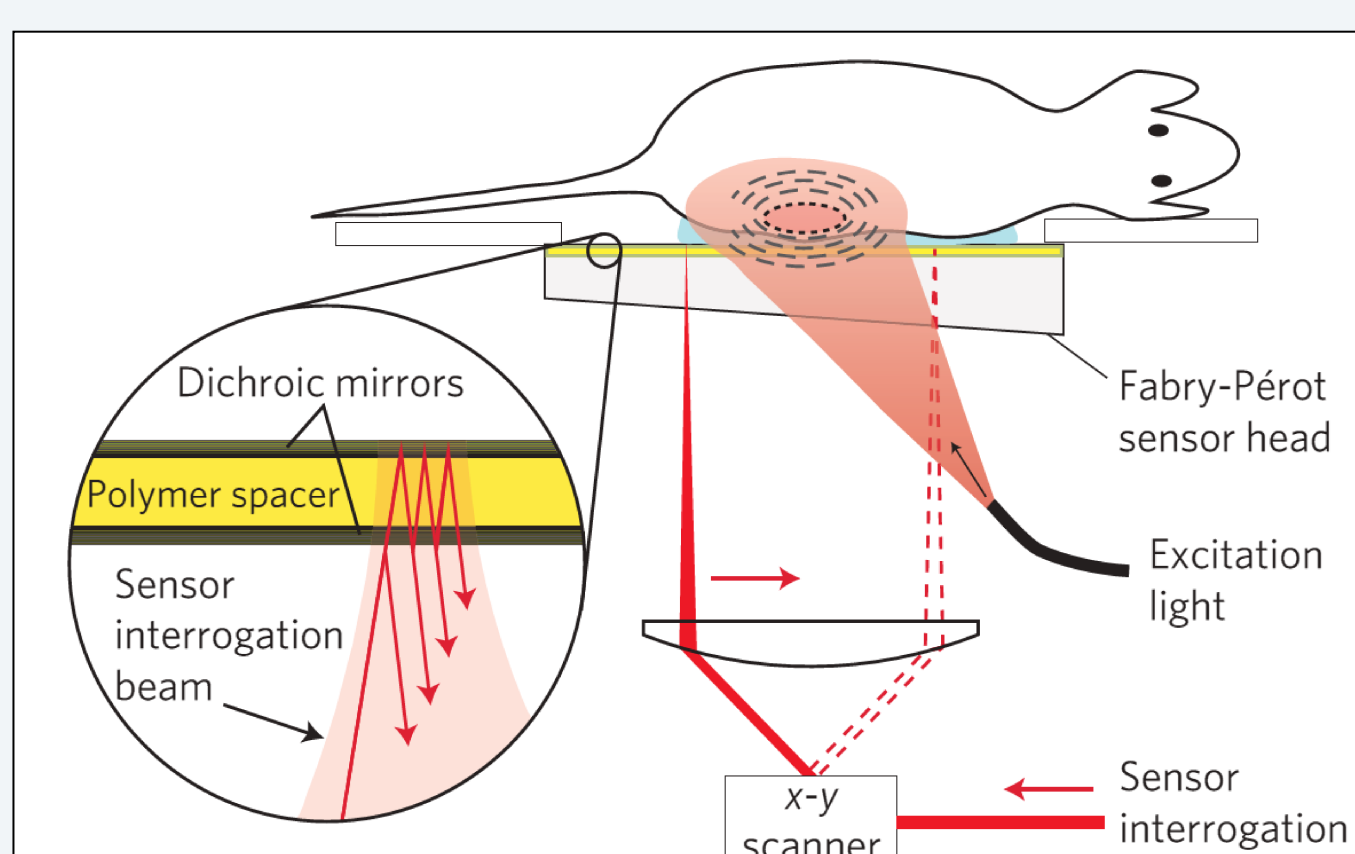


Fig. 1: Standard Fabry-Pérot (FB) scanners raster-sample the incident photoacoustic field sequentially with a high spatial resolution and sensitivity at the expense of a long acquisition time (cf. Zhang et al., 2008).

Sparse Variational Image Reconstruction

We need to solve $f = GAp_0$, with G sub-sampling and A forward operator. As conventional approaches fail when used on sub-sampled data (cf. Fig 4), we employ sparse variational regularization (e.g., *total variation*, *TV*),

$$\hat{p}_\lambda = \operatorname{argmin}_{p \geq 0} \frac{1}{2} \|f - GAp\|_2^2 + \lambda \mathcal{J}(p) \quad (1)$$

enhanced by *Bregman iterations* (Osher et al, 2005),

$$\hat{p}_\lambda^{k+1} = \operatorname{argmin}_{p \geq 0} \frac{1}{2} \|(f + b^k) - GAp\|_2^2 + \lambda \mathcal{J}(p)$$

$$b^{k+1} = b^k + f - GAp^{k+1}; \quad b_1 = 0$$

to compensate the systematic bias of (1) (cf. Fig 5).

Solving (1) by first order optimization schemes (Burger et al., 2014), requires to evaluate A and A^* . Our implementation relies on a *k*-space *pseudo-spectral method* for 3D acoustic wave propagation (Treeby & Cox, 2010) which utilizes GPU computing to cope with the immense computational challenges. We derived and examined an analytical representation of A^* in Arridge et al., 2016.

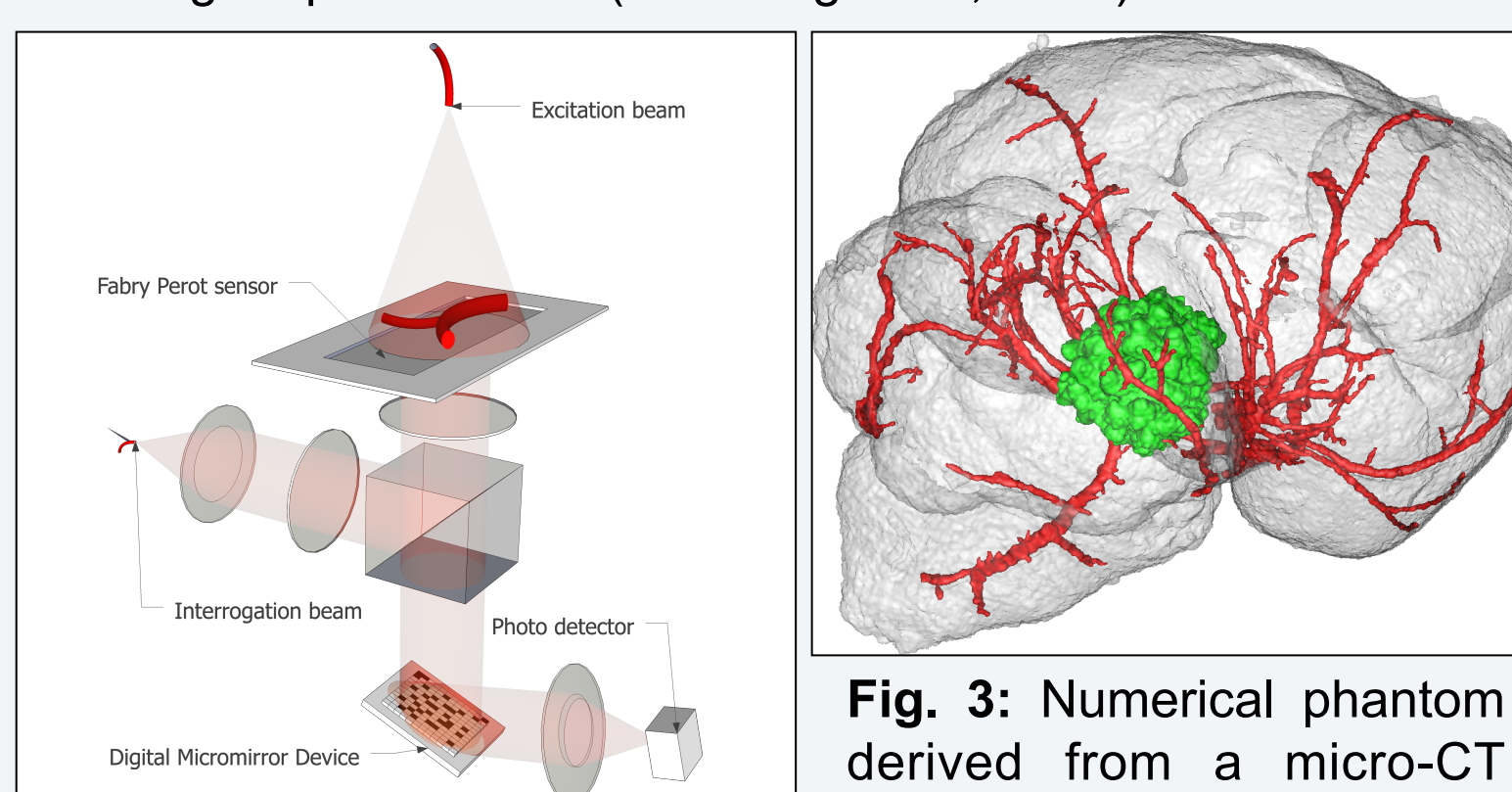


Fig. 2: Patterned interrogation: The interrogation laser is reflected from the FP sensor, patterned by the digital micromirror device and focused into a single photodiode (Huynh et al., 2014).

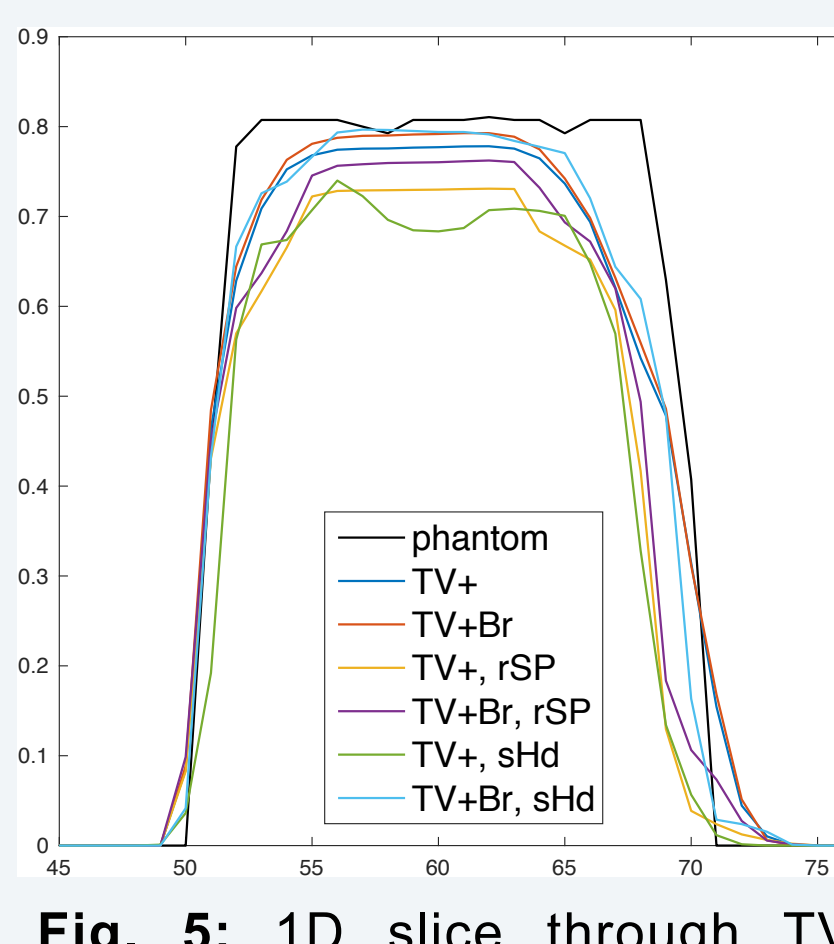


Fig. 5: 1D slice through TV regularization (TV+) and Bregman iterations (TV+Br) from Fig 4.

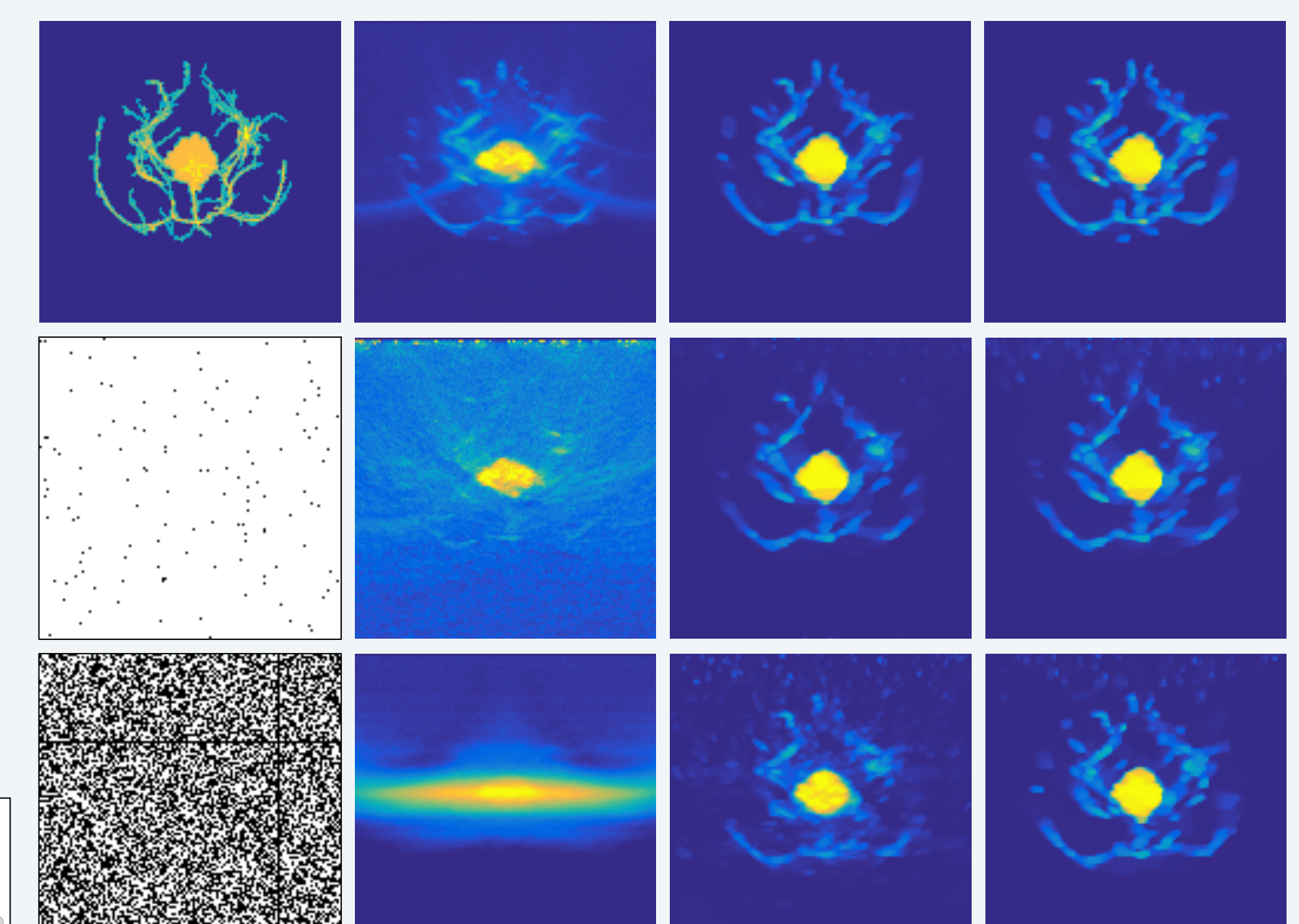


Fig. 4: "Best-case"-study: The phantom (Fig 3) is close to the detection plane (top edge), has a high contrast, all acoustic parameters are assumed known and the acoustic field is sampled at Nyquist frequency in space and time. Col 1: Maximum intensity projection (*mxIP*) of phantom and sketches of rSP and PT sub-sampling (acceleration factor 128 = 0.78% of the original data). Col 2-4: *mxIPs* of time reversal (TR, cf. Treeby & Cox, 2010), TV regularization and Bregman iterations for full data (row 1), rSP (row 2) and PI (row 3).

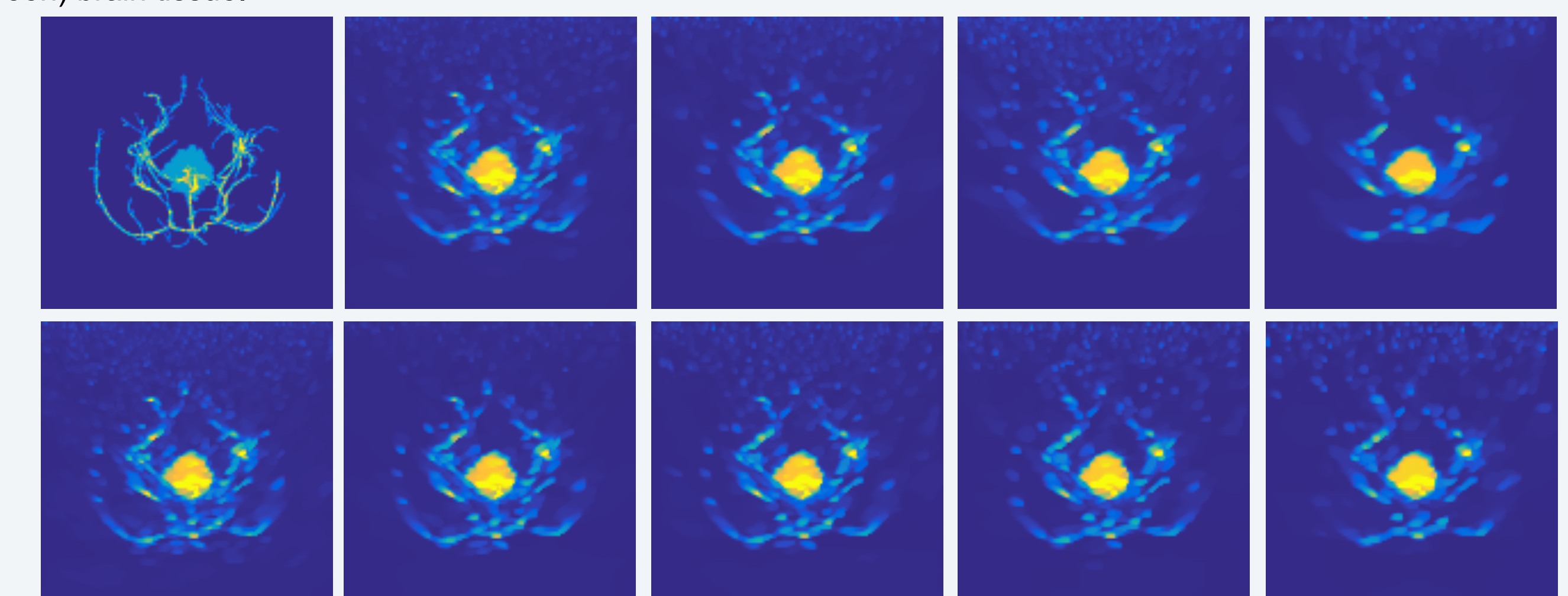


Fig. 6: "Realistic-case"-study: The phantom is more distant to the detection plane (top edge), has a lower contrast, the forward model is inaccurate and even for the "full" data, the acoustic field is spatially under-sampled. Col 1: *mxIP* of phantom and Bregman iteration for "full" data (i.e., regularly sub-sampled by a factor of 4). Col 2-5: *mxIPs* of Bregman iterations for rSP (row 1) and PI (row 2) sub-sampling with factors 1, 2, 4, 8 (col 2, 3, 4, 5).

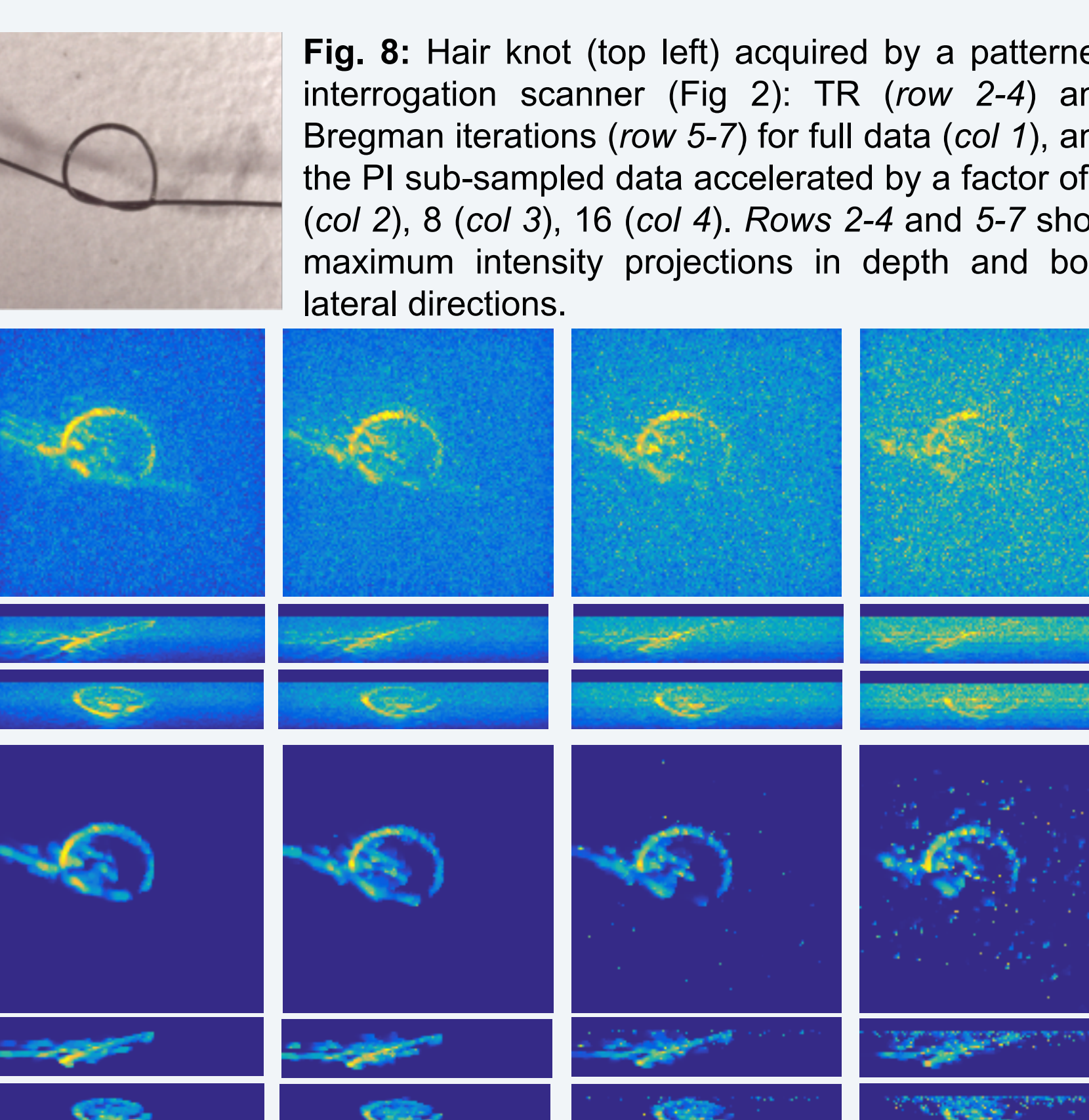


Fig. 8: Hair knot (top left) acquired by a patterned interrogation scanner (Fig 2): TR (row 2-4) and Bregman iterations (row 5-7) for full data (col 1), and the PI sub-sampled data accelerated by a factor of 4 (col 2), 8 (col 3), 16 (col 4). Rows 2-4 and 5-7 show maximum intensity projections in depth and both lateral directions.

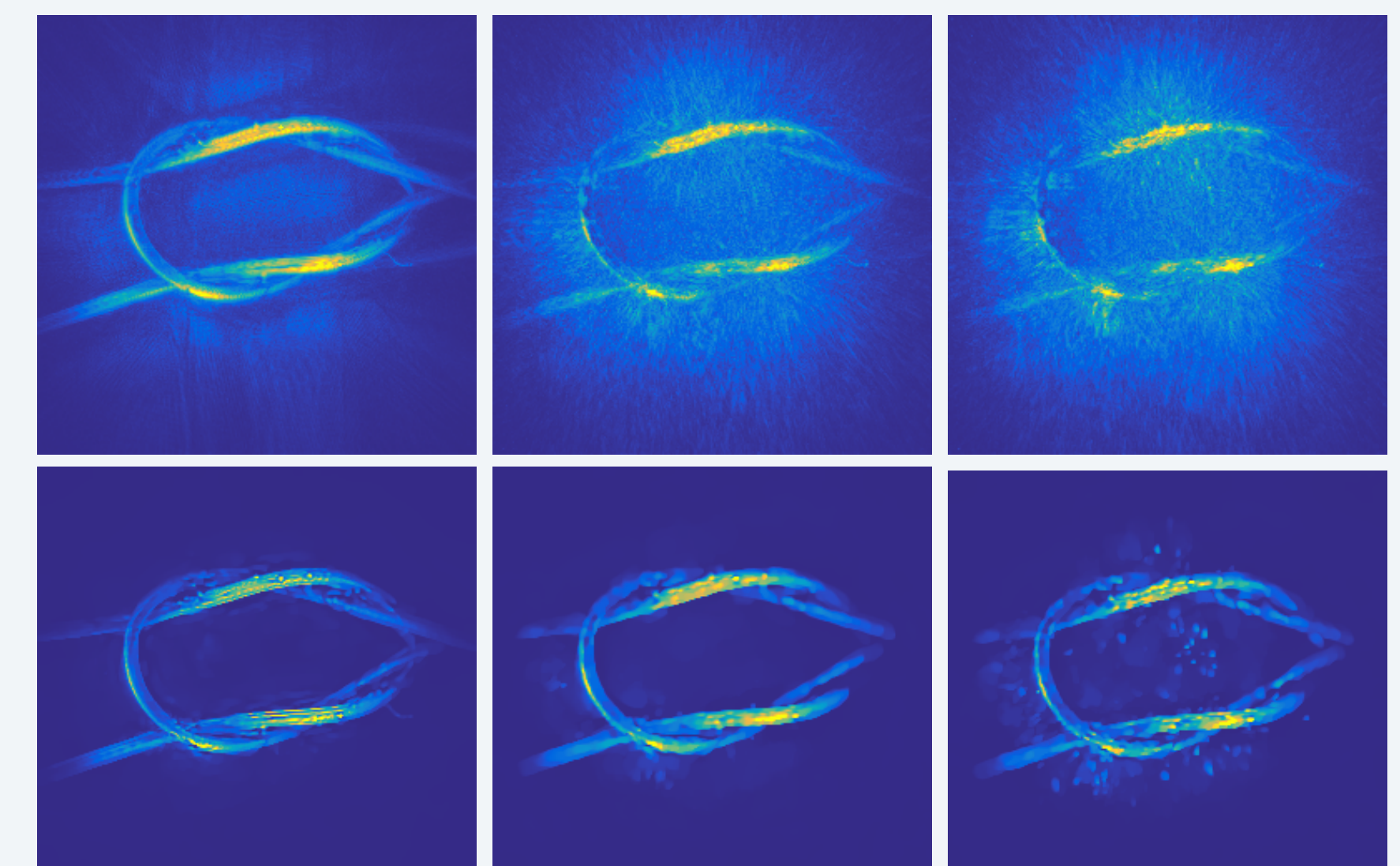


Fig. 7: Reconstructions of one frame of a dynamic experimental phantom: TR (row 1) and Bregman iterations (row 2) for full data (col 1) rSP sub-sampling by a factor of 4 (col 2) and 8 (col 3).

Results and Discussion

We first evaluated our methods with simulated data from a realistic phantom (Fig 3): In general, using sparse variational methods is essential to obtain high quality reconstructions from sub-sampled data (Fig 4). The comparison between "best-case" (Fig 4) and "realistic-case" data (Fig 6) reveals that the acceleration factor achievable heavily depends on the quality of the data. Furthermore, PI slightly outperforms rSP sub-sampling. Fig 7,8,9 show the results for experimental data: The acceleration factors achievable are similar to the "realistic-case" simulation study: Various non-trivial difficulties such as developing pre-processing routines and more accurate forward models will have to be overcome to realize higher acceleration factors (> 8). Fig 9 also reveals that the TV regularization used here is not suitable to recover thin, vessel-like structures but tends to break them apart.

Conclusion and Outlook

PAT wave fields can be highly compressible but a substantial acceleration of current sequential PAT scanners requires:

- Variational image reconstruction employing spatial sparsity constraints matching the structure of the target. Typical PAT targets, such as vasculature-rich images, need more sophisticated regularization terms than TV.
- An accurate forward model well-aligned with the data. This requires refined data pre-processing, and data-driven model calibration.

Further acceleration of dynamic PAT requires variational methods employing spatio-temporal sparsity constraints which also exploit the temporal redundancy of data generated by dynamics of low complexity.

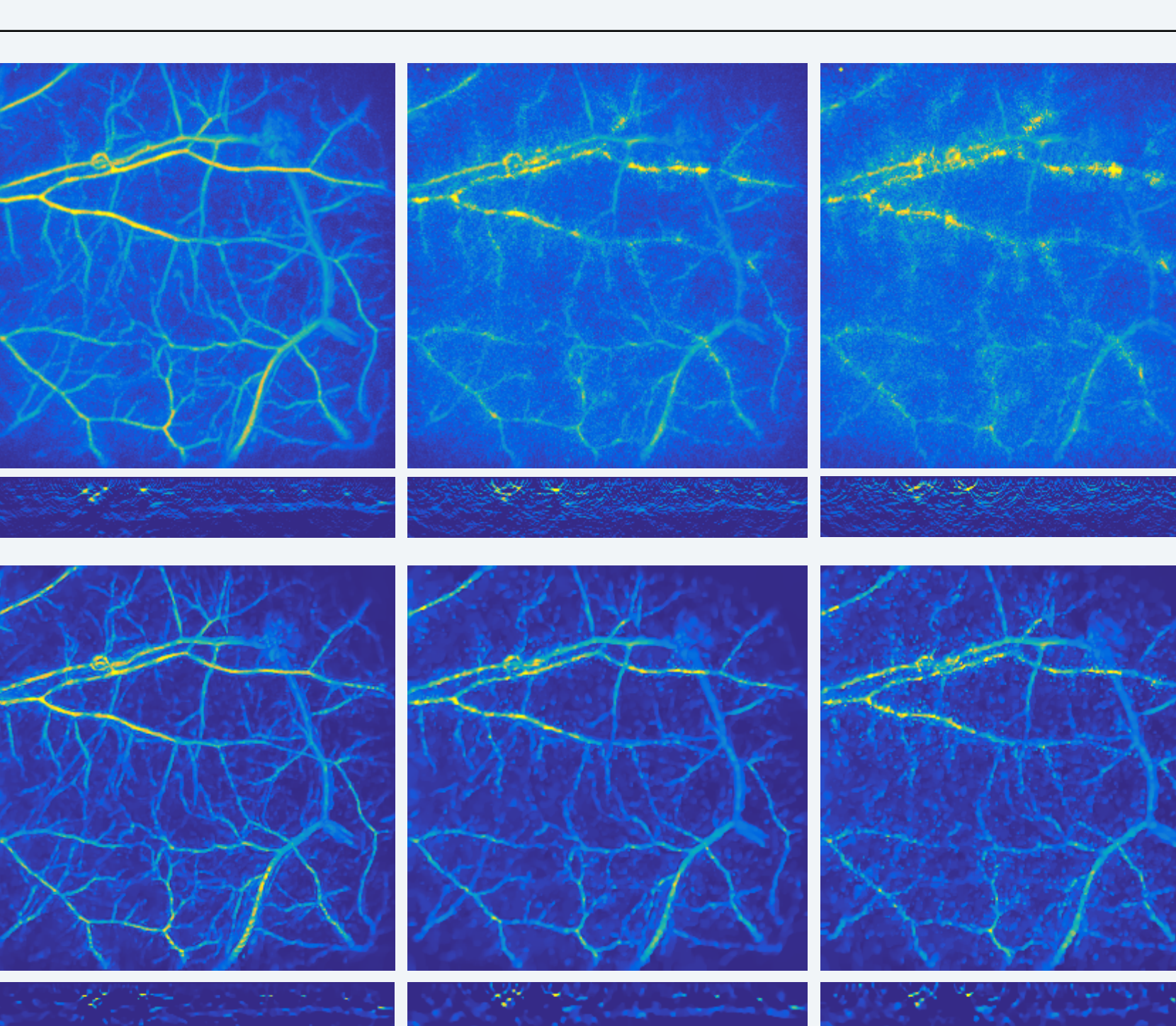


Fig. 9: In-vivo data of the skin vasculature of a mouse acquired by a standard FP scanner: Comparison between TR (row 1-2) and TVBreg (row 3-4) for full data (col 1), rSP sub-sampling by factor 4 (col 2) and 8 (col 3). Rows 1+3 show depth-mxIP, rows 2+4 a vertical slice.

- ## References & Acknowledgements
- Arridge, Betcke, Cox, Lucka, Treeby, 2016. On the Adjoint Operator in Photoacoustic Tomography. *arXiv:1602.02027*.
 - Burger, Sawatzky, Steidl, 2014. First Order Algorithms in Variational Image Processing, *arXiv:1412.4237*.
 - Huynh, Zhang, Betcke, Arridge, Beard Cox, 2014. Patterned interrogation scheme for compressed sensing photoacoustic imaging using a Fabry Perot planar sensor, *Proc. SPIE*, 8943.
 - Osher, Burger, Goldfarb, Xu, Yin, 2006. An iterative regularization method for total variation-based image restoration, *Multiscale Modeling and Simulation*, 2(4).
 - Zhang, Laufer, Beard, 2008. Backward-mode multi-wavelength photoacoustic scanner using a planar fabry-perot polymer film ultrasound sensor for high-resolution three-dimensional imaging of biological tissues, *Applied Optics*, 47(4).
 - Treeby, Cox, 2010. k-Wave: MATLAB toolbox for the simulation and reconstruction of photoacoustic wave fields, *Journal of Biomedical Optics*, 2(15).

We gratefully acknowledge the support of NVIDIA Corporation with the donation of the Tesla K40 GPU used for this research.

